

See discussions, stats, and author profiles for this publication at: <https://www.researchgate.net/publication/267925736>

# Novel Synthesis of Gold Nanoparticles Supported on AlkyneFunctionalized Nanosilica

ARTICLE *in* THE JOURNAL OF PHYSICAL CHEMISTRY C · OCTOBER 2014

Impact Factor: 4.77 · DOI: 10.1021/jp507637m

---

CITATIONS

2

---

READS

61

## 8 AUTHORS, INCLUDING:



[Maria Cristina Cassani](#)

University of Bologna

60 PUBLICATIONS 682 CITATIONS

[SEE PROFILE](#)



[Silvia Fazzini](#)

University of Bologna

6 PUBLICATIONS 21 CITATIONS

[SEE PROFILE](#)



[Barbara Ballarin](#)

University of Bologna

83 PUBLICATIONS 1,295 CITATIONS

[SEE PROFILE](#)



[Adriana Mignani](#)

University of Bologna

27 PUBLICATIONS 289 CITATIONS

[SEE PROFILE](#)

# Novel Synthesis of Gold Nanoparticles Supported on Alkyne-Functionalized Nanosilica

Silvia Fazzini,<sup>†</sup> Maria Cristina Cassani,<sup>\*,†</sup> Barbara Ballarin,<sup>†</sup> Elisa Boanini,<sup>‡</sup> Jean Sébastien Girardon,<sup>§</sup> Anne-Sophie Mamede,<sup>§</sup> Adriana Mignani,<sup>||</sup> and Daniele Nanni<sup>\*,†</sup>

<sup>†</sup>Dipartimento di Chimica Industriale “Toso Montanari”, Università di Bologna, Viale del Risorgimento 4, I-40136 Bologna, Italy

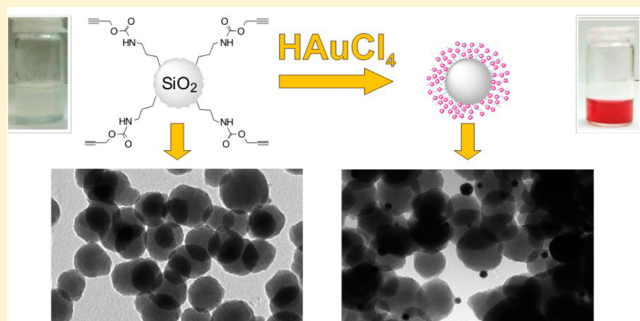
<sup>‡</sup>Dipartimento di Chimica “Giacomo Ciamician”, Università di Bologna, Via Selmi 2, I-40126 Bologna, Italy

<sup>§</sup>Unité de Catalyse et de Chimie du Solide, UMR CNRS 8181, Université Lille Nord de France, F-59655 Villeneuve d’Ascq Cedex, France

<sup>||</sup>Center for Industrial Research - Advanced Applications in Mechanical Engineering and Materials Technology (CIRI-MAM), University of Bologna, Viale del Risorgimento 2, I-40136 Bologna, Italy

## Supporting Information

**ABSTRACT:** A novel, convenient method for the preparation of gold nanoparticles supported on alkyne-functionalized nanosilica is presented. Silica nanoparticles functionalized with alkynyl carbamate moieties ( $\text{SiO}_2@\text{Yne}$ ) were synthesized by co-condensation of the difunctional organosilane [3-(2-propynylcarbamate)propyl]triethoxysilane (PPTEOS) with tetraethoxysilane (TEOS) in an alkaline medium. The alkynyl-carbamate functionalities present on silica are able to capture the gold precursor  $\text{HAuCl}_4$ , spontaneously reduce it, and stabilize the resulting supported  $\text{Au}_{\text{NPs}}$ , having an average size of ca. 11 nm. The prepared  $\text{Au}-\text{SiO}_2@\text{Yne}$  was thoroughly analyzed by X-ray photoelectron spectroscopy (XPS), thermogravimetric analysis (TGA), transmission electron microscopy (TEM), atomic absorption spectroscopy (AAS), FT-IR, and UV-vis spectroscopy. The catalytic activity of  $\text{Au}-\text{SiO}_2@\text{Yne}$  was investigated for the reduction of 4-nitrophenol to 4-aminophenol by  $\text{NaBH}_4$ , and kinetic constants  $k$  in the order of magnitude of about  $10^{-2} \text{ s}^{-1}$  were found.



## 1. INTRODUCTION

Silica is an attractive material due to its large abundance, stability, commercial availability, low cost, and ease of processing. Moreover, it finds widespread applications in technological fields such as optical devices, catalysts, and fillers for polymers.<sup>1</sup> The synthesis of colloidal silica by the Stöber method produces highly monodisperse spherical silica nanoparticles with a size ranging from 6 to 2000 nm.<sup>2</sup> This synthesis can be tailored as to cover different kinds of nanoparticles (NPs), such as gold,<sup>3–6</sup> silver,<sup>7</sup> and iron oxide,<sup>8,9</sup> with a silica layer, and can also be used as a direct method to obtain silica-functionalized nanoparticles by simply adding a suitably substituted alkoxy-silane bearing incondensable units to the mixture of tetraethoxysilane (TEOS) and ammonia (*co-condensation method*).<sup>10</sup> Functionalized silica can also be obtained by a postsynthetic method (*grafting*)<sup>11</sup> that involves further reaction of surface hydroxyl groups with organo-silane bearing various functional groups: this method typically results in inhomogeneous surface coverage where only part of those hydroxyl groups has been exploited. On the whole, the *co-condensation* method yields instead stable hybrid organo-silica NPs with a homogeneous distribution of the organic functionalities (such as amine,<sup>12</sup> fluorescent dyes,<sup>13</sup> carbazole,<sup>14</sup>

and alkyne<sup>15</sup> moieties) onto the silica nanoparticles. Both techniques are however widely used to prepare silica-supported gold catalysts by anchoring to the silica surface functionalities that possess strong affinity for gold (e.g., thiols, amines, etc.) and are positively charged, hence avoiding mobility and aggregation of the  $\text{Au}_{\text{NPs}}^{16}$ .

Recently, we reported the synthesis of stable silica-supported gold nanoparticles ( $\text{Au}/\text{SiO}_2\text{-PEI}$ ) suitable for catalysis, obtained by using, as the only reactants, chloroauric acid ( $\text{HAuCl}_4$ ) as the gold precursor and commercially available polyethylenimine-functionalized silica beads ( $\text{SiO}_2\text{-PEI}$ ), with the need for neither external reducing agents nor conventional stabilizing moieties.<sup>17</sup> The supported  $\text{Au}_{\text{NPs}}$  presented sizes in the range of 70–100 nm, with kinetic constants for reduction of 4-nitrophenol (4-NP) to 4-aminophenol (4-AP) in the presence of  $\text{NaBH}_4$  of the order of magnitude of  $1 \times 10^{-4} \text{ s}^{-1}$ .

In this work we describe the synthesis of silica nanoparticles functionalized with alkynyl carbamate moieties (hereafter termed  $\text{SiO}_2@\text{Yne}$ , Figure 1). The synergic effect of the

Received: July 29, 2014

Revised: October 1, 2014

Published: October 1, 2014

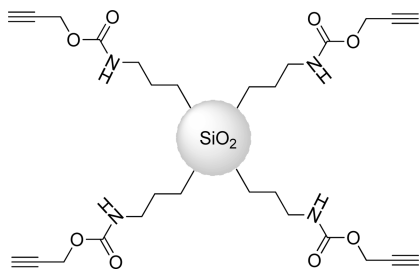


Figure 1. Alkyne-modified silica nanoparticle ( $\text{SiO}_2@\text{Yne}$ ).

carbamate and alkynyl functionalities present on the silica surface was exploited for the smooth reduction of  $\text{HAuCl}_4$  and successive stabilization of the resulting silica-supported  $\text{Au}_{\text{NPs}}$  ( $\text{Au-SiO}_2@\text{Yne}$ ). With respect to the  $\text{Au/SiO}_2\text{-PEI}$  system, these  $\text{Au}_{\text{NPs}}$  present an average size significantly smaller (11 nm) and a notably increased catalytic activity, with kinetic constants for reduction of 4-nitrophenol (4-NP) of 2 orders of magnitude higher.

## 2. EXPERIMENTAL SECTION

**2.1. Materials.** 3-(Triethoxysilyl)propyl isocyanate (IP-TEOS) (95%), tetraethoxysilane (TEOS) (99%), propargyl alcohol (99%), ethanol (99%), dichloromethane (DCM, 99%), triethylamine (TEA, 99%), sodium borohydride (98%), 4-nitrophenol (4-NP), and hydrochloric acid (HCl, 37 wt %) were of analytical grade and were used as purchased from Aldrich. Ammonia solution (30 wt %,  $d = 0.904 \text{ g/mL}$ ) and nitric acid ( $\text{HNO}_3$ , 65 wt %) were purchased from Carlo Erba. Ultrapure water purified with the Milli-Q plus system (Millipore Co., resistivity over 18  $\text{M}\Omega \text{ cm}$ ) was used in all cases.  $\text{HAuCl}_4\text{-}3\text{H}_2\text{O}$  was prepared as reported previously;<sup>18</sup> [3-(2-propynylcarbamate)propyl]triethoxysilane (3, PPTEOS) was prepared according to a literature procedure,<sup>15</sup> and details regarding the synthesis and characterization can be found in the Supporting Information (SI). The solids used for atomic absorption spectroscopy (AAS) measurements and catalytic tests were weighted with a Mettler Toledo AT 21 Comparator balance. All glassware was cleaned before use by immersion in aqua regia for several hours, rinsed with doubly ultrapure water and acetone, and dried in an oven.

**2.2. Preparation of Alkyne-Modified Silica Nanoparticles ( $\text{SiO}_2@\text{Yne}$ ).**  $\text{SiO}_2@\text{Yne}$  was obtained modifying a reported procedure.<sup>15</sup> Two syntheses were performed under nitrogen at 40 °C using two different concentrations of ammonia solution.

$\text{SiO}_2@\text{Yne-a}$ . A 100 mL two-neck dry round-bottom flask was charged with TEOS (2.0 mL, 9.4 mmol) and 50 mL of EtOH. PPTEOS (0.67 g, 2.2 mmol), previously dissolved in 15 mL of EtOH, was added to the vigorously stirred mixture. Once the system reached the desired temperature, ammonia (10 mL, 77 mmol) was added to the solution. After 2 min the solution became gradually milky white, which corresponds to the silica nanoparticle formation. The reaction mixture was allowed to stir for 24 h at 40 °C. After the reaction was completed, the obtained  $\text{SiO}_2@\text{Yne-a}$  was isolated by centrifugation (7800 rpm, 1 h) and redispersed in EtOH (20 mL) using an ultrasonic bath. The redispersion/centrifugation procedure was repeated three times.

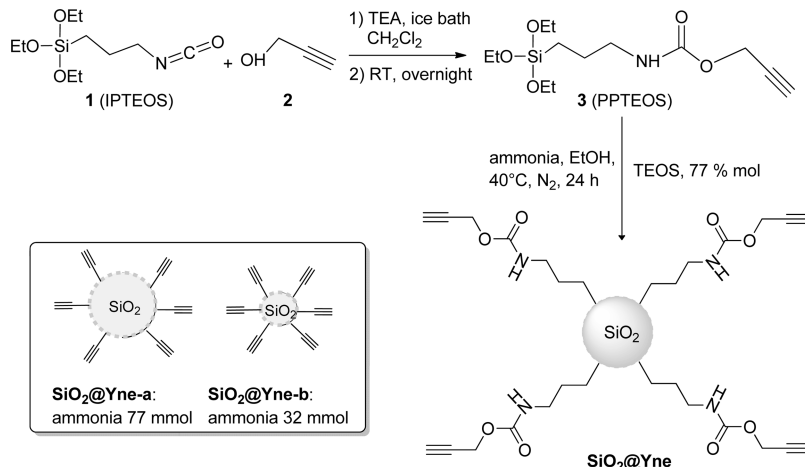
$\text{SiO}_2@\text{Yne-b}$ . Same procedure as with  $\text{SiO}_2@\text{Yne-a}$  but with a different ammonia amount (4.2 mL, 32 mmol).

The  $\text{SiO}_2@\text{Yne}$  dispersions can be conserved in EtOH and stored in the dark at 4 °C. In order to determine the NP concentration, 1 mL of dispersion was evaporated and dried, and the residue was weighed.  $\text{SiO}_2@\text{Yne}$  can be also conserved as a dried powder. For this purpose, the sample was concentrated under reduced pressure, dried in an oven at 50 °C for 3 h, and kept under a nitrogen stream to remove the residual solvent, resulting in a white powder. For the subsequent reactions the dried powders of  $\text{SiO}_2@\text{Yne}$  were always used to avoid precipitation of nanoparticles with change in concentration.

The samples **bare-SiO<sub>2</sub>-a** and **bare-SiO<sub>2</sub>-b** were prepared by the same procedure using TEOS (2 mL, 9.4 mmol) and different ammonia amounts (77 and 32 mmol, respectively).

**2.3. Synthesis of Au-SiO<sub>2</sub>@Yne.** Identical procedures were used for both  $\text{SiO}_2@\text{Yne-a}$  and  $\text{SiO}_2@\text{Yne-b}$ . Typically, in a 50 mL Pyrex glass immersed in an ultrasonic bath, 80 mg of functionalized silica and 20 mL of ultrapure water were added. After the first 10 min, needed to completely disperse the solid, 20 mL of 1 mM  $\text{HAuCl}_4$  was added. The reaction was carried out in the ultrasonic bath for 1 h, maintaining a constant temperature of 30 °C. After the first 10 min an initial violet color appeared that gradually changed into red-purple. At the end of the reaction, the obtained  $\text{Au-SiO}_2@\text{Yne}$  was separated by centrifugation at 5000 rpm for 30 min and redispersed twice in water and twice in EtOH using sonication. The collected functionalized silica was dried by an intense flux of  $\text{N}_2$  and kept in the oven for 4 h at 50 °C.

**2.4. Instruments.** Thermogravimetric analyses were carried out using a PerkinElmer TGA-7. Heating was performed in a platinum crucible at a rate of 10 °C/min from 40 to 900 °C. The sample weights were in the range 5–10 mg. XPS analyses were performed using a Kratos Analytical AXIS Ultra<sup>DLD</sup> spectrometer, equipped with a monochromatized aluminum source ( $\text{Al K}\alpha = 1486.6 \text{ eV}$ ) used for excitation. The analyzer was operated in a constant pass energy of 40 eV using an analysis area of approximately 700  $\mu\text{m} \times 300 \mu\text{m}$ . Charge compensation was applied to compensate for the charging effect occurring during the analysis. The Si 2p, O 1s, N 1s, and C 1s spectral regions were recorded. The quantification and decomposition of these experimental photopeaks were carried out using the CasaXPS software taking into account a background subtraction. As the spectral background is flat enough, the two methodologies based either on a Shirley background subtraction or on a linear background subtraction are equivalent. In this work, the second was preferred. DLS and  $\zeta$ -potential measurements were performed in ethanolic or aqueous dispersions using a Malvern Zetasizer Nano series Nano SZ. For TEM investigations a Philips CM 100 transmission electron microscope operating at 80 kV was used. To prepare the sample a drop of the suspension was transferred onto holey carbon foils supported on conventional copper microgrids. The amount of gold present on the different samples was determined with flame atomic absorption spectroscopy (AAS, Thermo Scientific) in air–acetylene flame with a wavelength of 242.8 nm and a spectral bandwidth of 0.5 nm. The analyses were conducted both on the supernatant solutions (indirect method) and on the solid samples (direct method) immediately after the end of the reaction, by comparison with calibration lines (direct method:  $y = 0.0392x + 0.0077$ ,  $R^2 = 0.9993$ ; indirect method:  $y = 0.0370x + 0.0166$ ,  $R^2 = 0.9975$ ). The standards for the direct method were prepared by dilution to 25 mL of different amounts of a

Scheme 1. Synthesis of  $\text{SiO}_2@\text{Yne}$ 

concentrated  $\text{HAuCl}_4$  aqueous solution with the addition of 6.5 mL of  $\text{NaOH}$  and 2 mL of aqua regia, whereas the standards for the indirect methods were prepared simply by dilution of a concentrated  $\text{HAuCl}_4$  aqueous solution with water. The supernatant solution was separated by centrifugation at 3000 rpm for 15 min by an Amicon Ultra centrifuge filter (cutoff: 100 kDa) and analyzed without further treatment. The solid sample (ca. 8 mg) was first dissolved at  $60^\circ\text{C}$  in a  $\text{NaOH}$  aqueous solution (2 M, 1 mL), and then 2 mL of aqua regia was added. Further 5.5 mL of 2 M  $\text{NaOH}$  was added to avoid silica precipitation, and finally it was diluted with water to a volume of 25 mL. The data obtained with the direct and indirect methods were identical within the experimental errors.

**2.5. Catalytic Reduction of 4-Nitrophenol (4-NP).** The catalytic activity of  $\text{Au-SiO}_2@\text{Yne}$  samples was examined in the reduction of 4-nitrophenol (4-NP) to 4-aminophenol (4-AP) in the presence of an excess of  $\text{NaBH}_4$  at  $25^\circ\text{C}$ . The details are reported in the SI.

### 3. RESULTS AND DISCUSSION

**3.1. Synthesis and Characterization of the Alkyne-Modified Silica Nanoparticles ( $\text{SiO}_2@\text{Yne}$ ).** The alkyne-terminated organosilane PPTEOS (3) was synthesized by a simple one-step addition of propargyl alcohol (2) to IPTEOS (1), catalyzed by triethylamine (TEA), to form the carbamate bond.<sup>19</sup> The alkyne functionality was hence introduced into the  $\text{SiO}_2$  network by a one-pot hydrolytic co-condensation of 3 (23% molar) and TEOS (77% molar) in basic medium at  $40^\circ\text{C}$  using a modified procedure (Scheme 1).<sup>15</sup>

By performing the synthesis with two different amounts of ammonia, two kinds of  $\text{SiO}_2@\text{Yne}$  were prepared:  $\text{SiO}_2@\text{Yne-a}$  and  $\text{SiO}_2@\text{Yne-b}$  (Scheme 1, inset). The former was obtained by adding 10 mL of ammonia (77 mmol) in the sol–gel preparation, leading to a 1 M final concentration in ammonia. The latter was instead obtained using 4.2 mL of ammonia (32 mmol) with a final concentration of 0.5 M. The bare silica nanoparticles (**bare-SiO<sub>2</sub>-a** and **bare-SiO<sub>2</sub>-b**) were prepared by the same procedure using TEOS and ammonia, without addition of PPTEOS.

The size and morphology of the two types of  $\text{SiO}_2@\text{Yne}$ , as well as that of the **bare-SiO<sub>2</sub>-a/b**, were determined by using TEM and DLS measurements. TEM images (Figure 2) showed a spherical geometry with a porous structure for both  $\text{SiO}_2@\text{Yne}$  samples, with an average size of  $79 \pm 23$  nm for  $\text{SiO}_2@\text{Yne-a}$

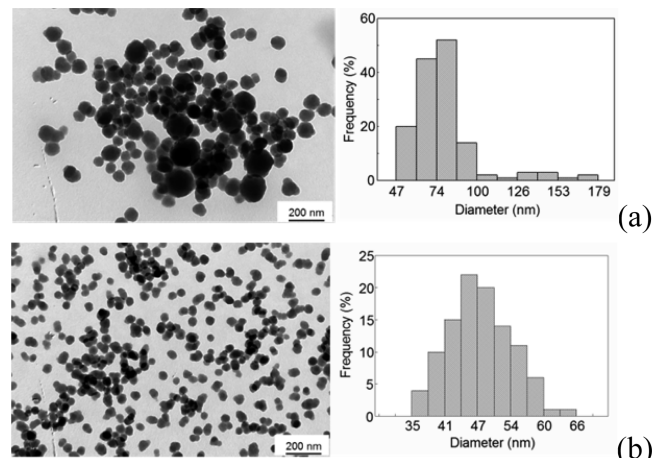


Figure 2. TEM images and size distributions: (a)  $\text{SiO}_2@\text{Yne-a}$  and (b)  $\text{SiO}_2@\text{Yne-b}$ .

**Yne-a** and  $45 \pm 6$  nm for **SiO<sub>2</sub>@Yne-b**, respectively (Table 1), where the average size was measured by counting 100

Table 1. DLS, TEM, and TGA results for  $\text{SiO}_2@\text{Yne-a/b}$

sample	wt % <sup>a</sup>	$d_{\text{DLS}}$ (nm) <sup>b</sup>	$\zeta$ -potential (mV)	$d_{\text{TEM}}$ (nm)
$\text{SiO}_2@\text{Yne-a}$	10%	$155 \pm 1$	$-58.9 \pm 5.9$	$79 \pm 23$
$\text{SiO}_2@\text{Yne-b}$	9%	$102 \pm 1$	$-46.2 \pm 5.8$	$45 \pm 6$

<sup>a</sup>Weight loss by TGA. <sup>b</sup>Z-average size.

nano particles from TEM images by the ImageJ software.<sup>20</sup> In agreement with what was reported by Stöber, by increasing ammonia concentration larger nanoparticles were obtained.<sup>2</sup> The ammonia concentration directly influenced both hydrolysis and condensation rate as highlighted by the appearance, after 2 min, of a milky white color in the preparation of  $\text{SiO}_2@\text{Yne-a}$  samples, whereas for  $\text{SiO}_2@\text{Yne-b}$  the same phenomenon was observed after 2 h. In the former case, high ammonia concentration quickly hydrolyzed the precursor, and hence rapid nucleation occurred. The fast nucleation process in  $\text{SiO}_2@\text{Yne-a}$ , together with the concomitant growth of the pre-existing nuclei, can justify the presence of another small population with an average size of ca. 150 nm. More monodispersed systems were instead obtained in  $\text{SiO}_2@\text{Yne-b}$ , where the slow hydrolysis resulted in smaller nanoparticles

with an average diameter of 45 nm (Figure 2b). TEM analysis performed on different batches showed a good reproducibility of size and morphology.

Using the same synthesis conditions as for  $\text{SiO}_2@\text{Yne-a/b}$  samples, the **bare-SiO<sub>2</sub>-a** and **bare-SiO<sub>2</sub>-b** exhibit an average size of  $367 \pm 32$  nm and  $77 \pm 7$  nm, respectively, hence larger than the modified ones (Table S1, SI). A comparison of the TEM micrographs of bare and functionalized silica is reported in the SI (Figure S5). This difference in dimensions between  $\text{SiO}_2@\text{Yne}$  and **bare-SiO<sub>2</sub>** can be explained in terms of a reduced number of propagating alkoxy groups in  $\text{SiO}_2@\text{Yne}$  during the hydrolysis step, which hinders particle growth and, in turn, leads to a decrease in size.<sup>21</sup>

The TGA analyses of  $\text{SiO}_2@\text{Yne-a/b}$  (Figure S7, SI) showed three regions of mass loss, 30–150 °C (adsorbed water and ethanol), 150–320 °C (organic material), and 400–730 °C (mainly dehydration of the SiOH group), and confirmed the successful incorporation of the alkynyl carbamate moiety with an additional 9–10% weight loss compared to **bare-SiO<sub>2</sub>-a/b** (Figure S6, SI). Finally, the presence of the alkyne group was also detected by FT-IR and Raman spectroscopy (Figures S8 and S9, SI).

The  $\text{SiO}_2@\text{Yne}$  aqueous dispersions were also investigated by DLS and  $\zeta$ -potential measurements. Since DLS analysis gives information on the inorganic core along with any coating material and the solvent layer attached onto the silica surface, the hydrodynamic radii found for all samples were larger than those measured by TEM. All the data discussed so far are summarized in Table 1.

The surface functionalization of the  $\text{SiO}_2@\text{Yne}$  was analyzed by XPS. The XPS survey spectra of  $\text{SiO}_2@\text{Yne-a}$  and  $\text{SiO}_2@\text{Yne-b}$ , which show all of the detectable elements present in the samples, are virtually identical: Figure 3 shows the spectrum of  $\text{SiO}_2@\text{Yne-a}$ .

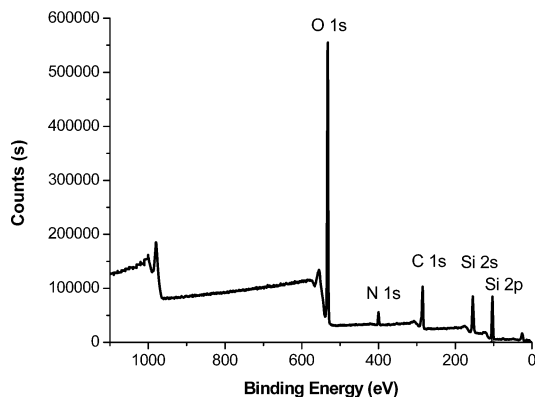


Figure 3. XPS survey spectrum of  $\text{SiO}_2@\text{Yne-a}$ .

The binding energies (BEs) and relative elemental compositions are reported in Table 2. It is worth noting that,

Table 2. XPS Elemental Quantification (Atomic %) for  $\text{SiO}_2@\text{Yne-a/b}$

element	BE (eV)	$\text{SiO}_2@\text{Yne-a}$ (at %)	$\text{SiO}_2@\text{Yne-b}$ (at %)
Si	$103.5 \pm 0.1$	19.2	22.1
O	$532.8 \pm 0.1$	49.8	51.0
N	$400.2 \pm 0.1$	3.8	3.1
C	$285.1 \pm 0.1$	27.2	23.8

in addition to silicon and oxygen, carbon and nitrogen, belonging to the organic functionalization, are also present. Table 2 shows that there are no significant differences, within the quantification error (~5%), between  $\text{SiO}_2@\text{Yne-a}$  and  $\text{SiO}_2@\text{Yne-b}$ . Concerning the bulk  $\text{SiO}_2$ , the observed O/Si atomic ratio (2.6 and 2.3, respectively) is slightly over the theoretical one (equal to 2) meaning a slight enrichment of surface oxygen. This difference could be explained by the oxygen coming from the surface functionalization and/or some surface pollution (residual adsorbed water).

The C 1s spectrum (Figure 4) was decomposed with three components centered at 285.0, 286.6, and 289.5 eV, which were assigned to C–C, C–H, and/or C–Si; C–N and/or C–O; and O=C=O bonds, respectively. The signal at 285.0 eV, attributed to C–C bonds, is generally affected by surface contamination due to sample air storage. By considering the percentage ratio of the areas under the well-separated peaks (C–C or C–O/N or O=C=O) with the total area of C 1s, the percentage distribution (C %) of each carbon chemical function was obtained (Figure 4).

By the ratio of these values with the O=C=O content, an idea of the different number of carbons present on the molecules anchored on the silica surface can be obtained (Table 3). These data are in agreement with the structure of condensed PPTEOS (Figure 5) for the C–N and C–O content. In the case of C–C the experimental ratio with O=C=O is slightly higher than the theoretical one. This fact can be the effect of contamination, which is always present, and it can also be ascribed to incomplete hydrolysis and condensation of the ethoxysilyl residues coming from the two organo-silane precursors (TEOS and PPTEOS), a phenomenon usually observed in the sol-gel synthesis.<sup>22</sup>

XPS analysis hence confirms, according to our previous results, that PPTEOS is anchored on the silica surface, giving in the meantime some reference data useful for analyzing the next synthetic step (*vide infra*).

### 3.2. Synthesis and Characterization of Au-SiO<sub>2</sub>@Yne.

The alkyne-modified silica-supported Au<sub>NPs</sub> ( $\text{Au-SiO}_2@\text{Yne}$ ) were prepared by simply adding an aqueous solution of HAuCl<sub>4</sub> (1 mM) to the same volume of a dispersion of  $\text{SiO}_2@\text{Yne-a}$  or  $\text{SiO}_2@\text{Yne-b}$  (2 mg/mL) in water in an ultrasonic bath for 1 h. The ultrasonic bath was used to avoid silica aggregation and to maintain the system homogeneous throughout the reaction. The amount of Au(III) precursor used was chosen in order to have a theoretical total amount of gold of 4.7 wt %. During the first 10 min the pale yellow color of the reaction mixture turned first to violet and then gradually to red-purple (Scheme 2, Figures S10 and S11, SI). At the end of the reaction, a portion of the crude material was directly analyzed by TEM, while the rest was separated by centrifugation and dried by an intense flux of N<sub>2</sub> in oven at 50 °C for 4 h to give  $\text{Au-SiO}_2@\text{Yne}$  as a purple powder, which was eventually thoroughly analyzed. It is worth noting that **bare-SiO<sub>2</sub>**, under the same reaction conditions, gave no change in color, even after months.

The Au content for both  $\text{Au-SiO}_2@\text{Yne-a}$  and  $\text{Au-SiO}_2@\text{Yne-b}$  was determined by AAS to be 4.7 wt %, i.e., equal to the total metal loading: this confirmed the absence of gold in the supernatant solutions and hence quantitative trapping by the functionalized silica. The UV-vis absorption spectra of both samples (Figure S12, SI) showed a surface plasmon resonance band (SPR) with maxima wavelength positions at 531 and 525 nm, respectively.

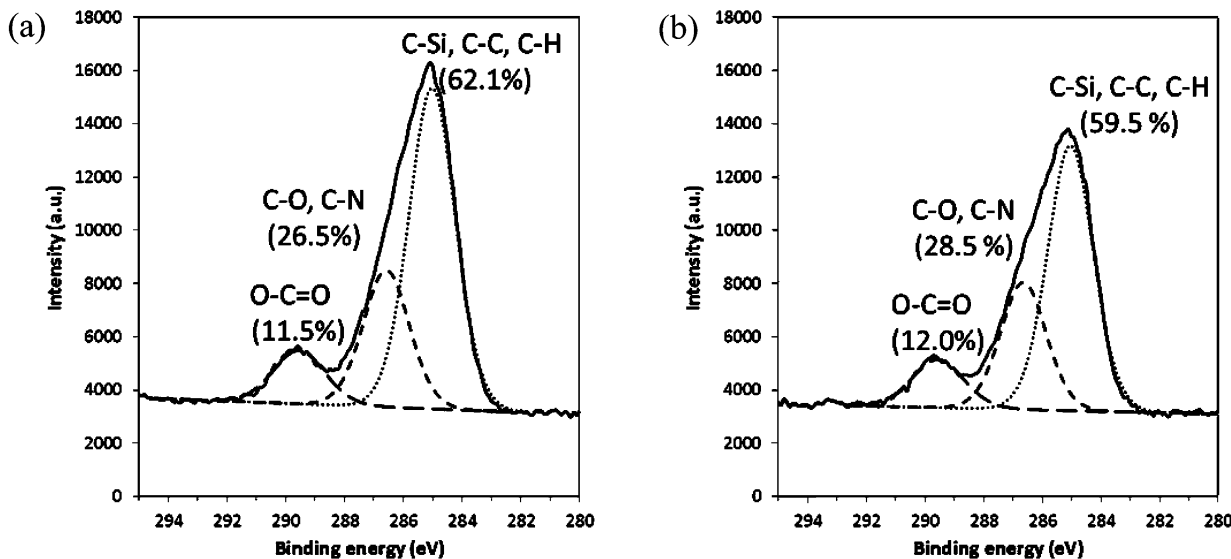


Figure 4. Spectral decomposition of the XPS C 1s photopeaks of (a)  $\text{SiO}_2@\text{Yne-a}$  and (b)  $\text{SiO}_2@\text{Yne-b}$ .

Table 3. Ratio of the Nitrogen and Carbon Chemical Functions with the O=C=O Content for  $\text{SiO}_2@\text{Yne-a/b}$

entry	ratio	$\text{SiO}_2@\text{Yne-a}$	$\text{SiO}_2@\text{Yne-b}$
1	NH/O-C=O	1	1
2	C-C/O-C=O	5	5
3	C-N, C-O/O-C=O	2	2

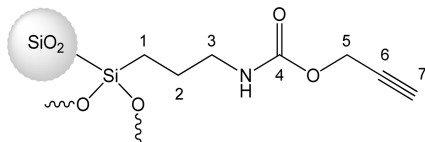


Figure 5. Alkyne-terminated silica containing three C–C (2 and 6), one C–Si (1), one C–H (7) [285.0 eV component], two C–N, C–O (3 and 5) [286.6 eV component], and one O=C=O (4) [289.5 eV component] bonds.

The morphology of  $\text{Au-SiO}_2@\text{Yne-a/b}$  samples was investigated by TEM microscopy (Figure 6). In both cases gold nanoparticles presented a spherical shape and were found attached onto the silica surface. Although the TEM analyses were carried out on the crude material prior to centrifugation, no free gold nanoparticles were detected, in agreement with AAS data. Sample  $\text{Au-SiO}_2@\text{Yne-a}$  showed supported  $\text{Au}_{\text{NPs}}$  with an average diameter of about  $15 \pm 3$  nm (Figure 6a), whereas TEM images of  $\text{Au-SiO}_2@\text{Yne-b}$  revealed the presence of nanoparticles with an average diameter of  $11 \pm 3$  nm (Figure 6b).

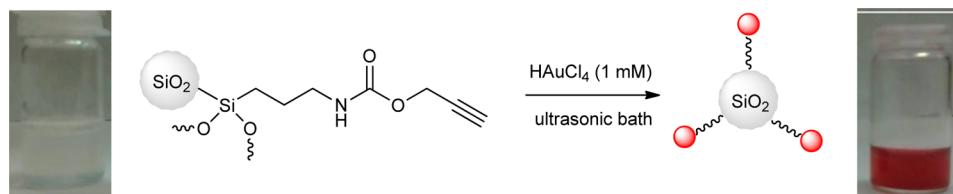
XPS survey spectra of the  $\text{Au-SiO}_2@\text{Yne}$  systems showed the same elements present in  $\text{SiO}_2@\text{Yne}$  and the appearance of a

new doublet ascribed to Au 4f with binding energies (BEs) of 84.3 and 88.3 eV, which are characteristic of metallic Au(0) species (Figure 7).<sup>23–25</sup> Table 4 reports the relative elemental compositions (%) for  $\text{Au-SiO}_2@\text{Yne-a/b}$ : both samples presented similar amounts of gold (0.5 and 0.4 at %, respectively). It is worth noting that only peaks ascribable to metallic gold were observed in both samples, and signals deriving from Au(I) and/or Au(III), expected at energies of around 85.5 and 86.5 eV, were not detected at all.

The C 1s peak was decomposed into four components, 285.0, 286.6, 289.6, and 288.4 eV, corresponding to C–C (C–H and C–Si), C–heteroatoms (C–O, C–N), O=C=O, and a new species or chemical function, respectively. This new component at 288.4 eV, not previously observed for  $\text{SiO}_2@\text{Yne}$  samples, was formed during reduction of Au(III) to Au(0). The percentage ratio in carbon (C %) of the decomposed chemical functions was considered and compared with the obtained values for the  $\text{SiO}_2@\text{Yne}$  samples (Table 5 and Figure 8).

A comparison between  $\text{Au-SiO}_2@\text{Yne}$  and  $\text{SiO}_2@\text{Yne}$  data shows, for the former, an evident decrease in O=C=O and C–C contents with a simultaneous increase in C–N and C–O and formation of a new species at 288.4 eV. As a general rule of the XPS technique, bonds with electronegative atoms lead to a shift toward higher binding energy (i.e., lower kinetic energy). The carbon in the carbamate ( $\text{H})\text{NC}(\text{O})\text{X}$  group, attached to electronegative atoms X such as oxygen and nitrogen, has a peak with a binding energy of 289.6 eV well distinguishable, by decomposition (Figure 8), from the new species found at 288.4 eV. The binding energy of the latter seems characteristic of a carbonyl species such as  $\text{RC}(\text{O})\text{R}'$ , in which R is a carbon and

Scheme 2. Synthesis of  $\text{Au-SiO}_2@\text{Yne}$



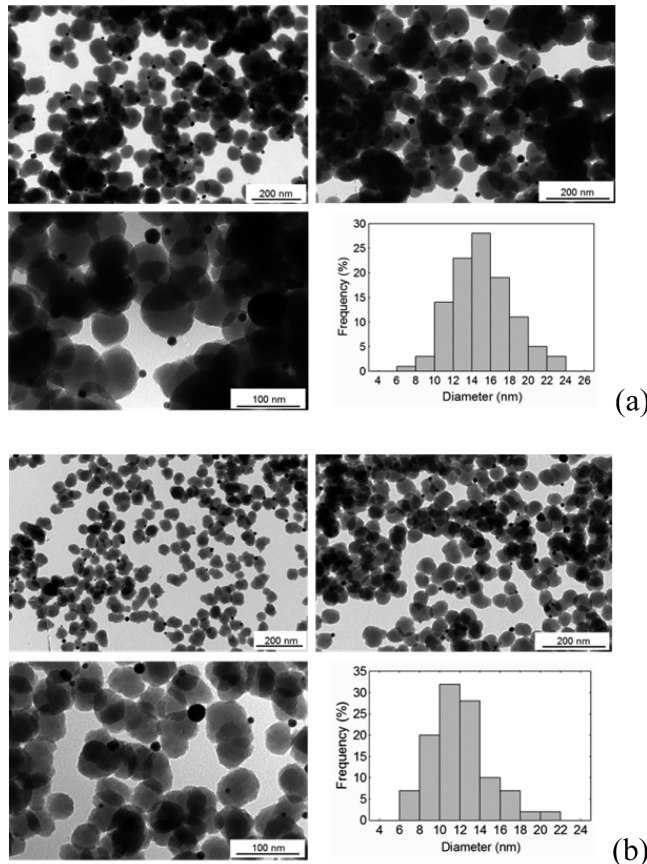


**Figure 6.** TEM images with size distribution histograms of supported  $\text{Au}_{\text{NPs}}$  in (a)  $\text{Au-SiO}_2@\text{Yne-a}$  and (b)  $\text{Au-SiO}_2@\text{Yne-b}$ .

$\text{R}'$  can be carbon or hydrogen, like in a ketone or an aldehyde.<sup>26</sup>

Reactions of alkynes with Au(III) substrates are well documented in the literature, and in general, partial reduction of Au(III) to Au(I) brings to mixed Au(III)/Au(I) complexes not as stable as the thiol and phosphine analogues.<sup>27</sup> Au(III) and Au(I) complexes can interact with the triple bond upon coordination and activate the alkyne moiety, which hence becomes more reactive toward nucleophiles.<sup>28–31</sup> For example,

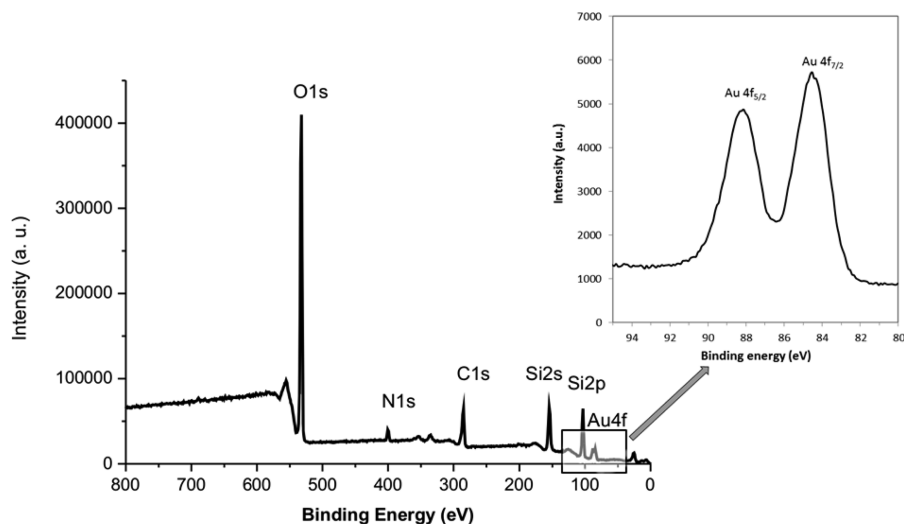
**Table 4.** XPS Atomic Percentage (at %) for  $\text{Au-SiO}_2@\text{Yne-a}/\text{b}$

element	BE (eV)	$\text{Au-SiO}_2@\text{Yne-a}$ (at %)	$\text{Au-SiO}_2@\text{Yne-b}$ (at %)
Si 2p	$103.3 \pm 0.1$	20.8	22.4
O 1s	$532.8 \pm 0.1$	50.4	50.3
N 1s	$400.1 \pm 0.1$	3.6	3.0
C 1s	$285.0 \pm 0.1$	24.7	23.9
Au 4f	$84.2 \pm 0.1$	0.5	0.4

Zhang<sup>32</sup> reported that systems similar to ours, such as propargyl esters (Scheme 3), undergo a great variety of chemical transformations catalyzed by Au(III) and Au(I) complexes. In his works<sup>33–35</sup> he has proposed different reaction mechanisms involving a structural rearrangement by either 1,2- or 1,3-acyl migrations to give an  $\alpha$ -vinyl gold oxocarbenium ion, as reported in Scheme 3.

Since in the reported studies no reduction to Au(0) was ever observed, we suppose that, in our system, the presence in the  $\text{SiO}_2@\text{Yne}$  of the carbamic nitrogen instead of the alkyl group R (the only notable distinction) could be the crucial difference capable of explaining our efficient formation of gold nanoparticles. A similar 1,3-migration mechanism was hence postulated involving the carbamic nitrogen (Scheme 4) with formation of the allene intermediate **A** followed by decarboxylation (to give **B**) and eventual rearrangement to the unsaturated imine **D**.

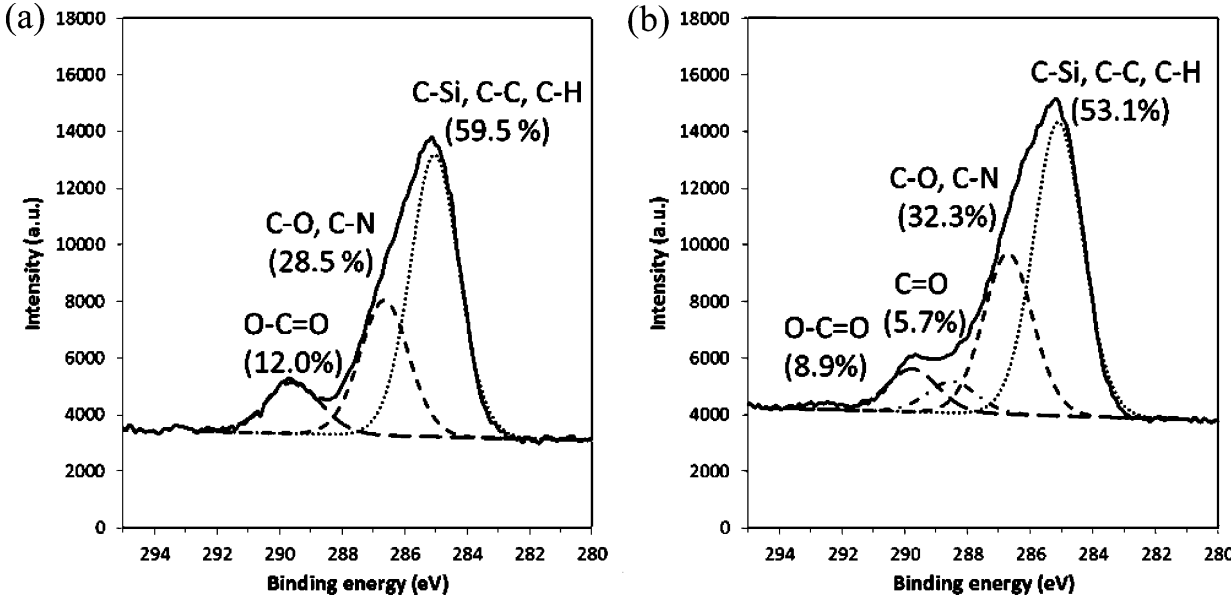
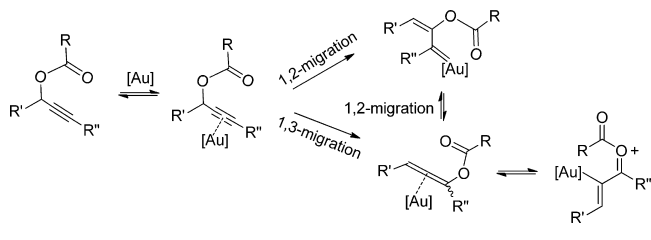
That imine, as well as its hydrolysis products (e.g., **E**), can act as an efficient reducing agent for Au(III) or Au(I) to  $\text{Au}_{\text{NPs}}$ , in analogy with the behavior observed for the previously reported nitrogen-containing systems ( $\text{Au/SiO}_2\text{-PEI}$ ).<sup>17</sup> Oxidation of the carbamate branch would eventually account, at the same time, for the formation of new carbonyl moieties (e.g., an aldehyde) on the silica, as shown by XPS data. Moreover, this tentative mechanism can explain the change in the percentage content of the total carbon with respect to the  $\text{SiO}_2@\text{Yne}$  samples. The FT-IR spectra of  $\text{Au-SiO}_2@\text{Yne-a}$  and **b** (Figure S13, SI) are very similar and show substantial changes compared to the  $\text{SiO}_2@\text{Yne}$  starting material: a loss in intensity of the bands at  $1660 \text{ cm}^{-1}$  ( $\nu \text{ C=O}$ ) and  $1538 \text{ cm}^{-1}$  ( $\delta \text{ N-H}$ ) was observed, and this was attributed to modifications that occurred to the carbamate group, where the formation of the



**Figure 7.** XPS survey spectra. Left panel:  $\text{Au-SiO}_2@\text{Yne-a}$  (full scale). Right panel: Au 4f level (same spectrum, expanded scale).

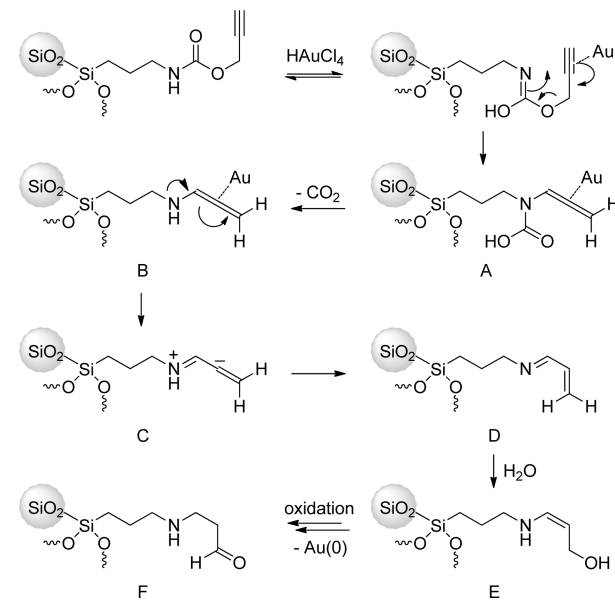
Table 5. Comparison between XPS C 1s Composition in  $\text{SiO}_2@\text{Yne}$  and  $\text{Au-SiO}_2@\text{Yne}$ 

C 1s	$\text{Au-SiO}_2@\text{Yne-a}$ (C %)	$\text{SiO}_2@\text{Yne-a}$ (C %)	$\text{Au-SiO}_2@\text{Yne-b}$ (C %)	$\text{SiO}_2@\text{Yne-b}$ (C %)
C 1s C—C, C—H	56.3	62.1	53.1	59.5
C 1s C—O, C—N	30.5	26.5	32.5	28.5
C 1s O—C=O	8.5	11.5	8.9	12
C 1s new peak	4.7	-	5.7	-

Figure 8. XPS C 1s spectra and chemical function distribution: (a)  $\text{SiO}_2@\text{Yne-b}$  and (b)  $\text{Au-SiO}_2@\text{Yne-b}$ .Scheme 3. Au(III)-Catalyzed Propargyl Ester Rearrangement ( $\text{R} = \text{H}, \text{CH}_2-\text{CH}_3$ )

final product F in Scheme 4 can also justify the decrease in intensity of the N—H bending since that bending vibration in amines is more difficult to be detected with respect to the N—H bond of carbamate.<sup>36</sup>

**3.3. Catalytic Activity.** The catalytic activity of  $\text{Au-SiO}_2@\text{Yne}$  was tested in the reduction of 4-nitrophenol (4-NP) to 4-aminophenol (4-AP) as a common benchmark reaction.<sup>17</sup> Organic nitro-compounds are very common chemicals, usually toxic for the environment, generated as byproducts in different industrial processes leading to agrochemicals, dyes, and drugs.<sup>37,38</sup> Among them, 4-nitrophenol (4-NP) is usually employed as a starting material for production of 4-aminophenol (4-AP), which is an important building block for the synthesis of different analgesics and drugs, e.g., paracetamol. In the majority of cases, the reduction of 4-NP to 4-AP occurs by use of a metal (generally iron) under acid conditions, a process, however, associated with great environmental hazards.<sup>39</sup> As a viable alternative, 4-NP can be converted into 4-AP via a metal-nanoparticle-catalyzed reduction with  $\text{NaBH}_4$ .<sup>40–49</sup> This procedure has already replaced the previous ones due to its straightforwardness and environmental conformity.

Scheme 4. Proposed Mechanism for the  $\text{SiO}_2@\text{Yne}$ -Mediated Reduction of  $\text{HAuCl}_4$ 

The catalytic reduction of 4-NP to 4-AP with an excess amount of  $\text{NaBH}_4$ , achievable neither in the absence of the catalyst (Figure S14, SI) nor with  $\text{SiO}_2@\text{Yne-a/b}$  only (Figure 9), was investigated for  $\text{Au-SiO}_2@\text{Yne-a/b}$  by using UV-vis spectroscopy (details are reported in the SI) with different 4-NP/ $\text{NaBH}_4$ /Au molar ratios (1/1560/1, 4/6250/1, and 10/15600/1). For both materials a total conversion of 4-NP to 4-AP was obtained in a few minutes (Figure 9 and Table 6).

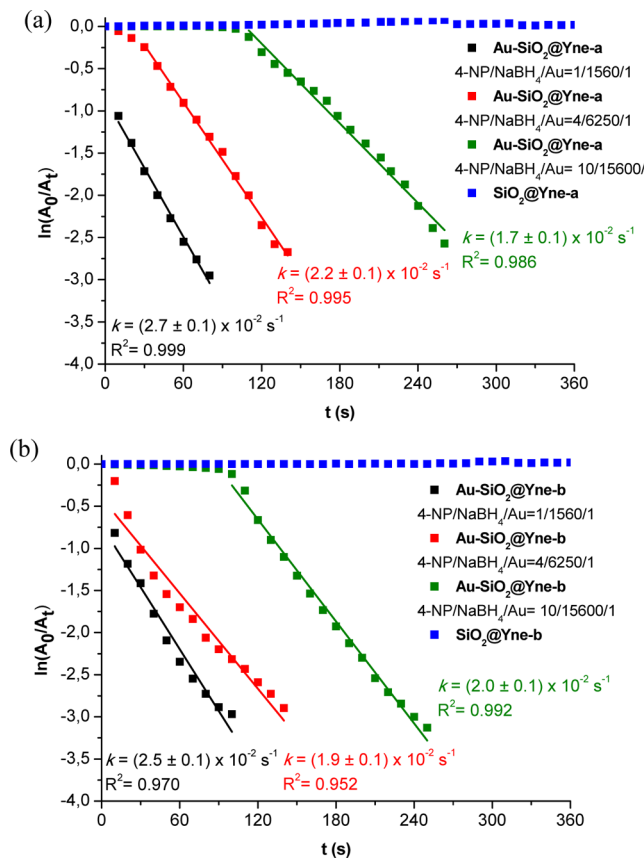


**Figure 9.** Plots of  $\ln(A_0/A_t)$  vs time for the reduction of 4-NP at different 4-NP/NaBH<sub>4</sub>/Au ratios for (a) Au-SiO<sub>2</sub>@Yne-a and (b) Au-SiO<sub>2</sub>@Yne-b. The plots of the functionalized silica without gold are also reported in each graph as a blank test (blue squares). Reaction conditions: aqueous media at 25 °C, 4-NP = 0.16 μmol, NaBH<sub>4</sub> = 0.25 mmol.

**Table 6. Calculated Kinetic Constants ( $k$ ) for 4-NP Reduction**

entry	sample	4-NP/NaBH <sub>4</sub> /Au (μmol/μmol/μmol)	$k$ ( $10^{-2} \text{ s}^{-1}$ )
1	Au-SiO <sub>2</sub> @Yne-a	1/1560/1	$2.7 \pm 0.1$
2	Au-SiO <sub>2</sub> @Yne-a	4/6250/1	$2.2 \pm 0.1$
3	Au-SiO <sub>2</sub> @Yne-a <sup>a</sup>	10/15600/1	$1.7 \pm 0.1$
4	Au-SiO <sub>2</sub> @Yne-b	1/1560/1	$2.5 \pm 0.1$
5	Au-SiO <sub>2</sub> @Yne-b	4/6250/1	$1.9 \pm 0.1$
6	Au-SiO <sub>2</sub> @Yne-b <sup>a</sup>	10/15600/1	$2.0 \pm 0.1$

<sup>a</sup>Presence of the induction period.

The calculated  $k$  values are 2 orders of magnitude higher than the ones obtained in our previous work, with the same gold content, for the Au/SiO<sub>2</sub>-PEI systems ( $k_{1/1660/1} = 1.14 \times 10^{-4} \text{ s}^{-1}$  under the same conditions).<sup>17</sup> They are also generally higher than the  $k$  values usually reported in the literature for

heterogeneous catalysts (usually in the order of magnitude of  $1 \times 10^{-3} \text{ s}^{-1}$ ),<sup>45,46,50</sup> and even comparable with  $k$  values typical of homogeneous catalysis.<sup>51</sup> The increased surface area of silica nanoparticles and the lower Au<sub>NPs</sub> average size (11 nm) justify the high catalytic performance of these systems. By decreasing the Au/4-NP ratio from 1/1 ( $\mu\text{mol}/\mu\text{mol}$ ) to 1/4 ( $\mu\text{mol}/\mu\text{mol}$ ), a slight decrease in the  $k$  values was detected for both Au-SiO<sub>2</sub>@Yne-a and Au-SiO<sub>2</sub>@Yne-b (Table 6, entries 1–2 and 4–5, respectively). Passing to a 1/10 ratio (Table 6, entries 3 and 6) an induction period of ca. 100 s was observed for both samples: under these conditions the very low amount of catalyst employed (0.066 mg) seemingly makes the diffusion rate of the substrate onto the catalyst a ruling factor for the reaction rate.<sup>51,52</sup>

The reusability of the immobilized metal nanoparticles in catalytic reactions is a standing challenge. In many cases, serious deactivation of the catalyst occurs within 2 to 5 cycles.<sup>44,46</sup> In our case the catalysts continue to show a high catalytic activity even after the fifth cycle (Table 7 and Figure 1S, SI).

#### 4. CONCLUSIONS

Silica nanoparticles functionalized with alkynyl carbamate moieties (SiO<sub>2</sub>@Yne) were synthesized by condensation of a difunctional organosilane, PPTEOS, with TEOS in alkaline medium. By simply performing the synthesis with different amounts of ammonia, two kinds of SiO<sub>2</sub>@Yne were prepared: SiO<sub>2</sub>@Yne-a and -b. Spherical alkyne-functionalized silica nanoparticles with a porous structure and different size distributions were obtained. In the case of SiO<sub>2</sub>@Yne-a (higher amounts of ammonia) the average size was  $79 \pm 23$  nm, whereas for SiO<sub>2</sub>@Yne-b (lower ammonia concentration) the average size was  $45 \pm 6$  nm. The most uniform particle size distribution was detected for SiO<sub>2</sub>@Yne-b.

By adding the obtained materials to an aqueous solution of HAuCl<sub>4</sub> spontaneous formation of Au<sub>NPs</sub> was observed in both cases and in very short times. Au<sub>NPs</sub> of about 15 and 11 nm anchored onto the silica surface were obtained with Au-SiO<sub>2</sub>@Yne-a and -b, respectively. XPS results revealed a change in structure of the carbamic functionality. Hence, a rearrangement mechanism triggered by Au(III) activation of the alkyne moiety with formation of an imine derivative was suggested. The final rearranged branch, eventually containing oxidizable groups, could account for the formation of both Au<sub>NPs</sub> and the novel carbonyl moieties (aldehydes) suggested by XPS data. The overall process would hence lead to a system capable of both reducing the Au(III) precursor and stabilizing the resulting Au<sub>NPs</sub> without the need for any additional agent preventing aggregation, similarly to what has been reported for Au/SiO<sub>2</sub>-PEI.<sup>17</sup> As far as we know, this is the first instance of efficient production of Au<sub>NPs</sub> by alkynyl-functionalized substrates.

These novel materials show very high activities for the reduction of 4-NP to 4-AP, with kinetic constants of the order of magnitude of  $1 \times 10^{-2} \text{ s}^{-1}$ . Hence, they are potentially

**Table 7. Kinetic Constants ( $k$ ) Obtained Using Fresh (First Cycle) and Recycled (Second to Fifth Cycle) Au-SiO<sub>2</sub>@Yne Catalysts with a 4-NP/NaBH<sub>4</sub>/Au Molar Ratio of 1/1560/1**

catalyst	first	second	third	fourth	fifth
Au-SiO <sub>2</sub> @Yne-a $k$ ( $10^{-2} \text{ s}^{-1}$ )	$2.7 \pm 0.1$	$2.7 \pm 0.1$	$2.9 \pm 0.2$	$2.2 \pm 0.1$	$2.1 \pm 0.1$
Au-SiO <sub>2</sub> @Yne-b $k$ ( $10^{-2} \text{ s}^{-1}$ )	$2.5 \pm 0.1$	$2.4 \pm 0.2$	$1.8 \pm 0.2$	$2.2 \pm 0.3$	$2.0 \pm 0.1^a$

<sup>a</sup>Presence of induction period.

powerful heterogeneous catalysts, with efficiencies comparable to homogeneous systems and a high level of reusability. Furthermore, they could represent a breakthrough among the “green” syntheses of supported gold nanoparticles since they would circumvent addition of both extra reducing agent and stabilizers, also allowing concomitant absorption of the active catalyst particles on the support immediately after spontaneous formation of gold nanoparticles.

As a final point, it is important to point out that  $\text{SiO}_2@\text{Yne}$  is a material susceptible of being easily further functionalized through its alkyne moiety (e.g., by click-chemistry approaches such as thiol/yne couplings),<sup>53,54</sup> both by the co-condensation or the grafting approach, yielding a range of novel analogous materials with in principle a huge variety of assorted properties, depending on the functionalization strategy. This point is currently under investigation.

## ASSOCIATED CONTENT

### Supporting Information

Experimental details for the synthesis and characterization of PPTEOS; additional TEM, TGA, FT-IR, and Raman characterizations for bare- $\text{SiO}_2$  and  $\text{SiO}_2@\text{Yne}$ ; additional UV-vis, FT-IR, and DLS characterization for Au- $\text{SiO}_2@\text{Yne}$ ; UV-vis spectra for the catalytic reduction of 4-NP and additional catalytic data. This material is available free of charge via the Internet at <http://pubs.acs.org>.

## AUTHOR INFORMATION

### Corresponding Authors

\*E-mail: maria.cassani@unibo.it (M.C.C.). Fax: +39 051 2093690. Tel.: +39 051 2093700.

\*E-mail: daniele.nanni@unibo.it (D.N.). Fax: +39 051 2093654. Tel.: +39 051 2093623.

### Notes

The authors declare no competing financial interest.

## ACKNOWLEDGMENTS

The authors wish to thank the University of Bologna and MIUR (PRIN 2010-2011-010PFLRJR, “PROxi” project) for financial support. A.M. thanks the Center for Industrial Research – Advanced Applications in Mechanical Engineering and Materials Technology (CIRI-MAM) for financial support. The Fonds Européen de Développement Régional (FEDER), CNRS, Région Nord Pas-de-Calais, and Ministère de l’Education Nationale de l’Enseignement Supérieur et de la Recherche are acknowledged for fundings of XPS/LEIS/Tof-SIMS spectrometers within the Pôle Régional d’Analyses de Surface. The authors also gratefully thank Dr. Alberto Mucchi for AAS measurements.

## REFERENCES

- (1) Silica. *Encyclopaedia Britannica. Encyclopaedia Britannica Online*; Encyclopaedia Britannica Inc., 2014. Web. 29 Jul. 2014. <http://www.britannica.com/EBchecked/topic/544154/silica>.
- (2) Stober, W.; Fink, A.; Bohn, E. Controlled Growth of Monodisperse Silica Spheres in the Micron Size Range. *J. Colloid Interface Sci.* **1968**, *26*, 62–69.
- (3) Wong, Y. J.; Zhu, L.; Teo, W. S.; Tan, Y.; Yang, Y.; Wang, C.; Chen, H. Revisiting the Stöber Method: Inhomogeneity in Silica Shells. *J. Am. Chem. Soc.* **2011**, *133*, 11422–11425.
- (4) Armelao, L.; Barreca, D.; Gasparotto, A.; Pierangelo, E.; Tondello, E.; Polizzi, S. Preparation of Gold Nanoparticles on Silica

Substrate by Radio Frequency Sputtering. *J. Nanosci. Nanotechnol.* **2005**, *5*, 259–265.

(5) Barreca, D.; Gasparotto, A.; Maccato, C.; Tondello, E. Silica-sandwiched Au Nanoparticle Arrays by a Soft PE-CVD/RF Sputtering Approach. *Nanotechnology* **2008**, *19*, 255602.

(6) Barreca, D.; Gasparotto, A.; Tondello, E. Metal/oxide Interfaces in Inorganic Nanosystems: What’s Going on and What’s Next? *J. Mater. Chem.* **2011**, *21*, 1648–1654.

(7) Shen, J.; Zhu, Y.; Yang, X.; Zong, J.; Li, C. Multifunctional  $\text{Fe}_3\text{O}_4@\text{Ag}/\text{SiO}_2/\text{Au}$  Core-Shell Microspheres as a Novel SERS-activity Label via Long-range Plasmon Coupling. *Langmuir* **2013**, *29*, 690–695.

(8) Sacanna, S.; Philipse, A. P. A Generic Single-Step Synthesis of Monodisperse Core/Shell Colloids Based on Spontaneous Pickering Emulsification. *Adv. Mater.* **2007**, *19*, 3824–3826.

(9) Caruana, L.; Costa, A. L.; Cassani, M. C.; Rampazzo, E.; Prodi, L.; Zaccheroni, N. Tailored  $\text{SiO}_2$ -Based Coatings for Dye Doped Superparamagnetic Nanocomposites. *Colloids Surf., A* **2012**, *410*, 111–118.

(10) Stein, A.; Melde, B. J.; Schroden, R. C. Hybrid Inorganic-Organic Mesoporous Silicates-Nanoscopic Reactors Coming of Age. *Adv. Mater.* **2000**, *12*, 1403–1419.

(11) Park, J.-W.; Park, Y. J.; Jun, C.-H. Post-Grafting of Silica Surfaces with Pre-functionalized Organosilanes: New Synthetic Equivalents of Conventional Trialkoxysilanes. *Chem. Commun.* **2011**, *47*, 4860–4871.

(12) Van Blaaderen, A.; Vrij, A. Synthesis and Characterization of Monodisperse Colloidal Organo-silica Spheres. *J. Colloid Interface Sci.* **1993**, *156*, 1–18.

(13) Peled, A.; Naddaka, M.; Lellouche, J.-P. Smartly Designed Photoreactive Silica Nanoparticles and their Reactivity. *J. Mater. Chem.* **2011**, *21*, 11511–11517.

(14) Peled, A.; Kotlyar, V.; Lellouche, J.-P. A New Method for the Preparation of Silica-Polycarbazole Composite Particles of a Core-Shell Morphology. *J. Mater. Chem.* **2009**, *19*, 268–273.

(15) Lu, X.; Sun, F.; Wang, J.; Zhong, J.; Dong, Q. A Facile Route to Prepare Organic/Inorganic Hybrid Nanomaterials by ‘Click Chemistry’. *Macromol. Rapid Commun.* **2009**, *30*, 2116–2120.

(16) Gutiérrez, L.-F.; Hamoudi, S.; Belkacemi, K. Synthesis of Gold Catalysts Supported on Mesoporous Silica Materials: Recent Developments. *Catalysts* **2011**, *1*, 97–154.

(17) Fazzini, S.; Nanni, D.; Ballarin, B.; Cassani, M. C.; Giorgietti, M.; Maccato, C.; Trapananti, A.; Aquilanti, G.; Ahmed, S. I. Straightforward Synthesis of Gold Nanoparticles Supported on Commercial Silica-Polyethyleneimine Beads. *J. Phys. Chem. C* **2012**, *116*, 25434–25443.

(18) Brauer, G. *Handbook of Preparative Inorganic Chemistry*; Academic Press: New York, 1963; Vol. II, p 1058.

(19) Choualeb, A.; Rosé, J.; Braunstein, P.; Welter, R. Routes to Ruthenium-Cobalt Clusters and Dicobalt Complexes with New Alkoxy-silyl- or Sulfur-Functionalized Alkynes. X-ray Structures of  $[\text{NEt}_4]^+[\text{RuCo}_3(\text{CO})_{10}\{\mu_4-\eta^2-\text{HC}_2(\text{CH}_2)_2\text{OC(O)NH(CH}_2)_3\text{Si(OEt)}_3\}]^-$  and  $[\text{Co}_2(\text{CO})_6\{\mu_2-\eta^2-\text{HC}_2\text{CH}_2\text{NHC(O)NH(CH}_2)_3\text{Si(OEt)}_3\}]^-$ . *Organometallics* **2003**, *22*, 2688–2693.

(20) ImageJ, Image processing and analysis in Java: <http://rsb.info.nih.gov/ij/>.

(21) Lee, J.; Lee, Y.; Youn, J. K.; Na, H. B.; Yu, T.; Kim, H.; Lee, S.-M.; Koo, Y.-M.; Kwak, J. H.; Park, H. G.; Chang, H. N.; Hwang, M.; Park, J.-G.; Kim, J.; Hyeon, T. Simple Synthesis of Functionalized Superparamagnetic Magnetite/Silica Core/Shell Nanoparticles and Their Application as Magnetically Separable High-Performance Biocatalysts. *Small* **2008**, *4*, 143–152.

(22) Wu, T.; Zhang, Q.; Hu, J.; Zhang, G.; Liu, S. Composite Silica Nanospheres Covalently Anchored with Gold Nanoparticles at the Outer Periphery of Thermo-responsive Polymer Brushes. *J. Mater. Chem.* **2012**, *22*, 5155–5163.

(23) Casaleto, M. P.; Longo, A.; Martorana, A.; Prestianni, A.; Venezia, A. M. XPS Study of Supported Gold Catalysts: the Role of

- $\text{Au}^0$  and  $\text{Au}^{+δ}$  Species as Active Sites. *Surf. Interface Anal.* **2006**, *38*, 215–218.
- (24) Brust, M.; Walker, M.; Bethell, D.; Schiffrin, D. J.; Whyman, R. Synthesis of Thiol Derivatised Gold Nanoparticles in a Two Phase Liquid/Liquid System. *J. Chem. Soc., Chem. Commun.* **1994**, 801–802.
- (25) Barreca, D.; Bovo, A.; Gasparotto, A.; Tondello, E. Au/SiO<sub>2</sub> Nanosystems by XPS. *Surf. Sci. Spectra* **2003**, *10*, 21–31.
- (26) Bhairamadgi, N. S.; Gangarapu, S.; Caipa Campos, M. A.; Paulusse, J. M. J.; van Rijn, C. J. M.; Zuilhof, H. Efficient Functionalization of Oxide-Free Silicon(111) Surfaces: Thiol-yne versus Thiol-ene Click Chemistry. *Langmuir* **2013**, *29*, 4535–4562.
- (27) Patai, S.; Rappoport, Z., Eds. *Chemistry of Organic Derivatives of Gold and Silver*; John Wiley & Sons Ltd: Chichester, UK, 1999.
- (28) Arcadi, A. Alternative Synthetic Methods through New Developments in Catalysis by Gold. *Chem. Rev.* **2008**, *108*, 3266–3325.
- (29) Hashmi, A. S. K. Gold-Catalyzed Organic Reactions. *Chem. Rev.* **2007**, *107*, 3180–3211.
- (30) Obradors, C.; Echavarren, A. M. Gold-Catalyzed Rearrangements and Beyond. *Acc. Chem. Res.* **2014**, *47*, 902–912.
- (31) Corma, A.; Leyva-Pérez, A.; Sabater, M. J. Gold-Catalyzed Carbon-Heteroatom Bond-Forming Reactions. *Chem. Rev.* **2011**, *111*, 1657–1712.
- (32) Wang, L.-J.; Zhu, H.-T.; Wang, A.-Q.; Qiu, Y.-F.; Liu, X.-Y.; Liang, Y.-M. Gold-Catalyzed Tandem [3,3]-Propargyl Ester Rearrangement Leading to (E)-1H-Inden-1-ones. *J. Org. Chem.* **2014**, *79*, 204–212.
- (33) Zhang, L. Tandem Au-Catalyzed 3,3-Rearrangement-[2 + 2] Cycloadditions of Propargylic Esters: Expedited Access to Highly Functionalized 2,3-Indoline-Fused Cyclobutanes. *J. Am. Chem. Soc.* **2005**, *127*, 16804–16805.
- (34) Li, G.; Zhang, G.; Zhang, L. Au-Catalyzed Synthesis of (1Z, 3E)-2-Pivaloxy-1,3-Dienes from Propargylic Pivalates. *J. Am. Chem. Soc.* **2008**, *130*, 3740–3741.
- (35) Shi, F.-Q.; Li, X.; Xia, Y.; Zhang, L.; Yu, Z.-X. A DFT Study of the Mechanisms of “In Water” Au(I)-Catalyzed Tandem [3,3] Rearrangement/Nazarov Reaction/[1,2]-Hydrogen Shift of Enynyl Acetates: A Proton-Transport Catalysis Strategy in the Water-Catalyzed [1,2]-Hydrogen Shift. *J. Am. Chem. Soc.* **2007**, *129*, 15503–15512.
- (36) Lin-Vien, D.; Colthup, N. B.; Fateley, W. G.; Grasselli, J. G., Eds. *The Handbook of Infrared and Raman Characteristic Frequencies of Organic Molecules*; Academic Press: New York, 1991.
- (37) Zheng, Y.; Ma, K.; Wang, H.; Sun, X.; Jiang, J.; Wang, C.; Li, R.; Ma, J. A Green Reduction of Aromatic Nitro Compounds to Aromatic Amines Over a Novel Ni/SiO<sub>2</sub> Catalyst Passivated with a Gas Mixture. *Catal. Lett.* **2008**, *124*, 268–276.
- (38) Swathi, T.; Buvaneswari, G. Application of NiCo<sub>2</sub>O<sub>4</sub> as a Catalyst in the Conversion of p-Nitrophenol to p-Aminophenol. *Mater. Lett.* **2008**, *62*, 3900–3902.
- (39) Sahiner, N.; Ozay, H.; Ozay, O.; Aktascı, N. A Soft Hydrogel Reactor for Cobalt Nanoparticle Preparation and Use in the Reduction of Nitrophenols. *Appl. Catal., B* **2010**, *101*, 137–143.
- (40) Chen, M.; Wang, C.; Fang, W.; Wang, J.; Zhang, W.; Jin, G.; Diao, G. Electrospinning of Calixarene-Functionalized Polyacrylonitrile Nanofiber Membranes and Application as an Adsorbent and Catalyst Support. *Langmuir* **2013**, *29*, 11858–11867.
- (41) Wang, H.; Dong, Z.; Na, C. Hierarchical Carbon Nanotube Membrane-Supported Gold Nanoparticles for Rapid Catalytic Reduction of p-Nitrophenol. *ACS Sustainable Chem. Eng.* **2013**, *1*, 746–752.
- (42) Peng, Y.; Wu, X.; Qiu, L.; Liu, C.; Wang, S.; Yan, F. Synthesis of Carbon–PtAu Nanoparticle Hybrids Originating from Triethoxysilane-Derivatized Ionic Liquids for Methanol Electrooxidation and the Catalytic Reduction of 4-Nitrophenol. *J. Mater. Chem. A* **2013**, *1*, 9257–9263.
- (43) Liu, B.; Zhang, W.; Feng, H.; Yang, X. Rattle-Type Microspheres as a Support of Tiny Gold Nanoparticles for Highly Efficient Catalysis. *Chem. Commun.* **2011**, *47*, 11727–11729.
- (44) Panigrahi, S.; Basu, S.; Praharaj, S.; Pande, S.; Jana, S.; Pal, A.; Ghosh, S. K.; Pal, T. Synthesis and Size-Selective Catalysis by Supported Gold Nanoparticles: Study on Heterogeneous and Homogeneous Catalytic Process. *J. Phys. Chem. C* **2007**, *111*, 4596–4605.
- (45) Ballarin, B.; Cassani, M. C.; Tonelli, D.; Boanini, E.; Albonetti, S.; Blosi, M.; Gazzano, M. Gold Nanoparticle-Containing Membranes from in Situ Reduction of a Gold(III)-Aminoethylimidazolium Aurate Salt. *J. Phys. Chem. C* **2010**, *114*, 9693–9701.
- (46) Kuroda, K.; Ishida, T.; Haruta, M. Reduction of 4-Nitrophenol to 4-Aminophenol Over Au Nanoparticles Deposited on PMMA. *J. Mol. Catal. A* **2009**, *298*, 7–11.
- (47) Huang, X.; Liao, X.; Shi, B. Synthesis of Highly Active and Reusable Supported Gold Nanoparticles and Their Catalytic Applications to 4-Nitrophenol Reduction. *Green Chem.* **2011**, *13*, 2801–2805.
- (48) Schrinner, M.; Polzer, F.; Mei, Y.; Lu, Y.; Haupt, B.; Ballauff, M.; Göldel, A.; Drechsler, M.; Preussner, J.; Glatzel, U. Mechanism of the Formation of Amorphous Gold Nanoparticles within Spherical Polyelectrolyte Brushes. *Macromol. Chem. Phys.* **2007**, *208*, 1542–1547.
- (49) Liu, J.; Qin, G.; Raveendran, P.; Ikushima, Y. Facile “Green” Synthesis, Characterization, and Catalytic Function of β-D-Glucose-Stabilized Au Nanocrystals. *Chem.—Eur. J.* **2006**, *12*, 2131–2138.
- (50) Lin, Y.; Qiao, Y.; Wang, Y.; Yan, Y.; Huang, J. Self-assembled Laminated Nanoribbon-Directed Synthesis of Noble Metallic Nanoparticle-Decorated Silica Nanotubes and Their Catalytic Applications. *J. Mater. Chem.* **2012**, *22*, 18314–18320.
- (51) Ishida, T.; Kuroda, K.; Kinoshita, N.; Minagawa, W.; Haruta, M. Direct Deposition of Gold Nanoparticles onto Polymer Beads and Glucose Oxidation with H<sub>2</sub>O<sub>2</sub>. *J. Colloid Interface Sci.* **2008**, *323*, 105–111.
- (52) Hayakawa, K.; Yoshimura, T.; Esumi, K. Preparation of Gold–Dendrimer Nanocomposites by Laser Irradiation and Their Catalytic Reduction of 4-Nitrophenol. *Langmuir* **2003**, *19*, 5517–5521.
- (53) Minozzi, M.; Monesi, A.; Nanni, D.; Spagnolo, P.; Marchetti, N.; Massi, A. An Insight into the Radical Thiol/Yne Coupling: The Emergence of Arylalkyne-Tagged Sugars for the Direct Photoinduced Glycosylation of Cysteine-Containing Peptides. *J. Org. Chem.* **2011**, *76*, 450–459.
- (54) Massi, A.; Nanni, D. Thiol–Yne Coupling: Revisiting Old Concepts as a Breakthrough for Up-To-Date Applications. *Org. Biomol. Chem.* **2012**, *10*, 3791–3807.